



CHORUS

This is the accepted manuscript made available via CHORUS. The article has been published as:

Photoionization of $\text{Fe}^{\{7+\}}$ from the ground and metastable states

S. S. Tayal and O. Zatsarinny

Phys. Rev. A **91**, 013413 — Published 26 January 2015

DOI: [10.1103/PhysRevA.91.013413](https://doi.org/10.1103/PhysRevA.91.013413)

Photoionization of Fe^{7+} from the ground and metastable states

S. S. Tayal*

Department of Physics, Clark Atlanta University, Atlanta, GA 30314, USA

O. Zatsarinny†

Department of Physics and Astronomy, Drake University, Des Moines, IA, 50311, USA

The B -spline Breit-Pauli R -matrix method is used to investigate the photoionization of Fe^{7+} from the ground and metastable states in the energy region from ionization thresholds to 172 eV. The present calculations were designed to resolve the large discrepancies between the recent measurements and available theoretical results. The multiconfiguration Hartree-Fock method in connection with B -spline expansions is employed for an accurate representation of the initial and final states wave functions. The close-coupling expansion includes 99 fine-structure levels of the residual Fe^{8+} ion in energy region up to $3s^23p^54s$ states. It includes levels of the $3s^23p^6$, $3s^23p^53d$, $3s^23p^54s$, and $3s3p^63d$ configurations and some levels of the $3s^23p^43d^2$ configuration which lie in the energy region under investigation. The present photoionization cross sections in the length and velocity formulations exhibit excellent agreement. The present photoionization cross sections agree well with the Breit-Pauli R -matrix calculation of Sossah et al. and the TOPbase data in the magnitude of the background nonresonant cross sections, but show somewhat richer resonance structure which qualitatively agree with the measurements. The calculated cross sections, however, are several times lower than the measured cross sections depending upon photon energy. The cross sections for photoionization of metastable states were found to have approximately the same magnitude as the cross sections for photoionization of the ground state, thereby, the presence of metastable states in the ion beam may not be the reason for enhancement of the measured cross sections.

PACS numbers: 32.80.Fb

I. INTRODUCTION

Photoionization of atoms and ions is one of the main elementary processes of the electromagnetic radiation interaction with matter, and the photoionization cross sections are of great significance in many applications such as plasma physics, lighting industry, atmospheric science, and several fields of astrophysics. The photoionization of ions, especially ions of the transition metals Ti, Mn, Fe, and Ni are also important in controlled thermonuclear fusion reactors. These metals appear as impurities from the fusion reactor walls, or they are deliberately released as diagnostic tracer elements. The photoionization processes of these ions directly effect cooling, transport, and confinement of plasma in different high temperature fusion devices. Absolute cross sections for photoionization of these ions are also of great interest to model spectral emissions from stellar atmospheres, novae, and active galactic nuclei.

Despite a long history of their calculations and measurements, the photoionization cross sections for many ions remain uncertain. In high-temperature plasma environments atoms can be found in different ionic states. Therefore, the plasma modeling requires studies of ionization and recombination processes along isonuclear sequences, i.e., for different ionic states of an element. Each

ion has its specific atomic structure and there is significant change along the isonuclear sequences when various filled subshells are opened. It produces extreme difficulty in both the theoretical studies of atomic structure and dynamical processes of these ions and interpretation of experimental measurements. Another complication arises from the fact that many ions at high temperatures have considerable population of metastable states. Usually, measurements can not provide the quantitative information on the metastable states in the ion beam, and thus normally does not allow direct comparison with theoretical cross sections.

Iron is among the most astrophysically abundant elements, and hence its ions can serve as a important diagnostic tool in different astrophysical environments. For this reason, iron ions received significant attention from both theory and experiment. Theoretically, photoionization of iron ions has been explored extensively as part of the Opacity Project [1] and Iron Project [2]. On the experimental side, photoionization measurements for iron ions were made using synchrotron radiation and an atomic-beam technique. The absolute single- and double-photoionization cross sections of singly charged Fe ions have been measured from 15.8 to 180 eV using the merged-beam technique [3]. Experimental and theoretical studies of the photoionization cross section of Fe^{4+} ion between 59 and 140 eV photon energy were reported by Bizau *et al.* [4]. The available R -matrix calculations describe qualitatively well the results of the experiment in the $3p \rightarrow 3d$ excitation region. Photoionization of Fe^{2+} through Fe^{6+} has been measured from their thresh-

*Electronic Address: stayal@cau.edu

†Electronic Address: oleg.zatsarinny@drake.edu

olds to 160 eV [5]. It was shown that the theoretical results tend to overestimate the intensity of the $3p \rightarrow 3d$ photoexcitations. In particular, an anomalously low value of the integrated oscillator strength is measured for Fe^{2+} ion. Recently, cross sections for single photoionization of Fe^{3+} , Fe^{5+} , and Fe^{7+} ions have been measured at high spectral resolutions of 0.04, 0.15, and 0.13 eV, respectively by Gharaibeh *et al.* [6]. Absolute photoionization cross-section measurements were also performed using ion beams containing undetermined fractions of ions in their ground and metastable states. It makes their interpretation and comparisons with theory and other measurements difficult. Nevertheless, considerable differences with available theoretical results were noted.

The theoretical studies of structure and dynamical processes in transition metal atoms and ions with open 3d subshells are both challenging and interesting as discussed by Sossah *et al.* [7]. They investigated photoionization of K-like ions ($Z = 22-26$) using both nonrelativistic and Breit-Pauli R -matrix methods. They calculated photoionization cross sections from the ground $3s^2 3p^6 3d^2 D_{3/2}$ and metastable $3s^2 3p^6 3d^2 D_{5/2}$ states and found substantial changes in the photoionization spectra of K-like ions as $3p \rightarrow 3d$ excitation moves from the continuum to the bound part of the spectrum for $Z \geq 23$. The $3p \rightarrow 3d$ excitation energy for Fe^{7+} lie below the 3d ionization threshold and thus the photoionization spectrum of Fe^{7+} contains weaker and narrower Rydberg series of resonances with excitation of 3p electron to autoionizing states with $n \geq 4$. As a result the sum of oscillator strengths in the continuum decreases with increasing Z from $Z = 21$ to $Z = 26$. In the photoionization of Ca^+ , Sc^{2+} , and Ti^{3+} the $3p \rightarrow 3d$ excitation energy is above the 3d threshold and the giant resonances occur due to the $3s^2 3p^6 3d^2 D - 3s^2 3p^5 3d^2 F^o$ transition which decay through a Super-Coster-Kronig $3s^2 3p^5 3d^2 - 3s^2 3p^6 + e$ transition. The measurements of Gharaibeh *et al.* [6] were performed after the calculations of Sossah *et al.* [7] and no comparison of the measured results was made with the calculations of Sossah *et al.* [7]. The primary objective of our work is to present a comparison of various calculations with experiment and to investigate possible cause of discrepancies.

II. CALCULATIONS

A. Target wave functions

The final residual ionic states of Fe^{8+} in the present calculations were generated by combining the multi-configuration Hartree-Fock (MCHF) and the B -spline box-based multichannel methods [8]. Specifically, the structure of the multichannel target expansions was cho-

sen as

$$\begin{aligned} \Phi^J = & \sum_{nl,LS} \{ \phi(3s^2 3p^5) P(nl) \}^{LSJ} \\ & + \sum_{nl,LS} \{ \phi(3s 3p^6) P(nl) \}^{LSJ} \\ & + a_{LSJ} \varphi(3s^2 3p^4 3d^2)^{LSJ} + b_{LSJ} \varphi(3s 3p^5 3d^2)^{LSJ} \end{aligned} \quad (1)$$

where $P(nl)$ denotes the wave function of the outer valence electron. First two terms in the above expansion represent the entire $3s^2 3p^5 nl$ and $3s 3p^6 nl$ Rydberg series in Fe^{8+} , while the $3d^2$ states are represented with individual configuration-interaction (CI) expansions φ . They can be considered as "perturbers" to the Rydberg series. The inner-core or short-range correlation is included through the CI expansion of the $\phi(3s^2 3p^5)$ and $\phi(3s 3p^6)$ ionic states. These expansions along with the perturber expansions φ were generated in separate multi-configuration calculations using the program MCHF [9]. The multiconfiguration expansions φ include all single and double promotions from the $3s$ and $3p$ orbitals to the $3d$ and $4\bar{l}$ ($l = 0 - 4$) correlated orbitals, which are generated separately for each configuration. In order to keep the final expansions for the final Fe^{8+} states to a reasonable size, all contributions with expansion coefficients of magnitude less than 0.02 were neglected. Note that we also used separate CI expansions for the initial ground and metastable states that allow us to include relaxation effects via state-specific one-electron orbitals.

The unknown functions $P(nl)$ for the outer valence electron were expanded in a B -spline basis, subject to the condition that the wave functions vanish at the boundary. The B -spline coefficients for the valence orbitals $P(nl)$, along with the coefficients $(a, b)_{LSJ}$ for the perturbers, were obtained by diagonalizing the atomic Breit-Pauli Hamiltonian, which include all one-electron relativistic corrections. The above scheme yields a set of term-dependent one-electron orbitals for each valence orbital, also accounting for important interactions between the Rydberg series and the perturbers. Since such multichannel bound-state calculations generate different non-orthogonal sets of orbitals for each atomic state, their subsequent use in photoionization calculations is somewhat complicated. On the other hand, our configuration expansions for the atomic target states contained from 400 to 600 configurations for each state and hence could be used in the photoionization calculations with available computational resources.

Table I contains the Fe^{8+} target states that were included in present photoionization calculations. The present calculated excitation energies are compared with the available experimental values from the NIST compilation [10] and other calculations. Storey *et al.* [11], Verma *et al.* [12], and Aggarwal *et al.* [13] reported energy levels and radiative rates for Fe^{8+} using well-tested computer codes. They considered different numbers of levels that were described by different CI expansions to account for electron correlation effects. Storey *et al.* [11] considered

140 levels of the $3s^23p^6$, $3s^23p^53d$, $3s^23p^54s$, $3s^23p^54p$, and $3s^23p^43d^2$ configurations in their SUPERSTRUCTURE [14] calculations and Verma *et al.* [12] included 87 levels of the $3s^23p^6$, $3s^23p^53d$, $3s^23p^54l$ ($l=0-3$), $3s3p^63d$, $3s3p^64s$, $3s3p^64p$, and $3s^23p^55l$ ($l=0-2$) configurations in the CIV3 structure calculation [15]. Aggarwal *et al.* [13] performed most extensive calculations using the fully relativistic GRASP [16] as well as the FAC [17] codes and carried out in-depth investigation of CI expansions by including various configurations of $n = 3$ and $n = 4$ complexes. They concluded that their GRASP results with 2471 levels are most accurate with the accuracy of energies for many levels better than 1%. We have included these results for comparison in Table I. The lower part of the Fe^{8+} spectrum consists 12 levels of the $3s^23p^53d$ configuration and 4 levels of the $3s3p^63d$ configuration. Energies of these levels are well-established experimentally and the present excitation energies agree closely with experimental energies in the range of 0.35 eV. The calculated energies of Aggarwal *et al.* [13] and Storey *et al.* [11] differ from the experimental energies by up to 1.56 eV except for the $3s^23p^53d \ ^1P_1^o$ level where the difference is about 2.1 eV. We note strong term-dependence of the 3d orbital for these levels, especially for the 1P term, which is directly included in the present calculations with non-orthogonal orbital technique. We also found very strong core-valence correlation for these levels due to $3p^2 - 3d^2$ promotion in the $3s^23p^33d^3$ and $3s3p^43d^3$ states and these are included in our CI expansions. Aggarwal *et al.* [13] also noted strong interaction between the $3s^23p^33d^3$ and $3s^23p^43d^2$ configurations.

Next comes levels of the $3s^23p^43d^2$ configuration in the Fe^{8+} spectrum. We have included 78 levels of the

$3s^23p^43d^2$ configuration and 4 levels of the $3s^23p^54s$ configuration in the description of final residual Fe^{8+} ion. The importance of the $3s^23p^43d^2$ levels has been discussed by Storey *et al.* [11], Aggarwal *et al.* [13], and Liedahl [18] on the overall accuracy of energy levels. The calculation of Verma *et al.* [12] did not include levels of the $3s^23p^43d^2$ configuration and this deficiency of their calculation has been discussed in details by Aggarwal *et al.* [13]. Only a few levels of this configuration are identified from the experimental measurements that can be used for benchmark comparison with theory. Young [19] proposed identification for the multiplet $3s^23p^4(^3P)3d^2(^1G) \ ^3G$ (indexes 96-98 in the Table I). Our calculations agree within 1.1 eV with his identifications, while the calculations of Aggarwal *et al.* [13] and Storey *et al.* [11] differ by about 4.90 and 5.38 eV, respectively. This agreement can be considered as reasonable, taking into account the rather strong restriction of CI expansions with cut-off factor of 0.02 was imposed in order to obtain feasible representation of target states in our subsequent R -matrix photoionization calculations. The present calculation as well as the calculations of Aggarwal *et al.* [13] and Storey *et al.* [11] are *ab initio* while Verma *et al.* [12] adjusted diagonal elements of the Hamiltonian matrices to bring their calculated energies close to the experimental values. The experimental energies are also available for the $3s^23p^54s \ ^3P_1$ and 1P_1 levels (indexes 91 and 99). The present excitation energies closely agree with experiment, with the same accuracy as for the $3s^23p^53d$ levels discussed above. The calculations of Aggarwal *et al.* [13] and Storey *et al.* [11] agree to about 3.20 and 4.80 eV, respectively.

TABLE I: Comparison of present level energies (eV) with measured values from NIST and calculated results of Aggarwal *et al.* [13] (A06) and Storey *et al.* [11] (S02). The difference between various calculated and experimental values are also given.

Index	Configuration	LSJ	NIST ^a	present	diff.	A06 ^b	diff.	S02 ^c	diff.
1	$3s^23p^6$	1S_0	0.00	0.00	0.00	0.00	0.00	0.00	0.00
2	$3s^23p^53d$	$^3P_0^o$	50.31	50.31	0.00	50.92	0.61	51.19	0.88
3	$3s^23p^53d$	$^3P_1^o$	50.62	50.64	0.02	51.24	0.62	51.54	0.92
4	$3s^23p^53d$	$^3P_2^o$	51.29	51.32	0.03	51.91	0.62	52.26	0.97
5	$3s^23p^53d$	$^3F_4^o$	52.79	53.05	0.25	53.69	0.90	53.96	1.17
6	$3s^23p^53d$	$^3F_3^o$	53.23	53.46	0.24	54.14	0.91	54.39	1.16
7	$3s^23p^53d$	$^3F_2^o$	53.79	54.00	0.21	54.70	0.92	54.96	1.17
8	$3s^23p^53d$	$^3D_3^o$	56.49	56.80	0.31	57.60	1.11	57.73	1.24
9	$3s^23p^53d$	$^1D_2^o$	56.63	56.86	0.23	57.80	1.17	57.91	1.28
10	$3s^23p^53d$	$^3D_1^o$	57.11	57.35	0.24	58.21	1.10	58.34	1.23
11	$3s^23p^53d$	$^3D_2^o$	57.36	57.59	0.23	58.48	1.12	58.64	1.29
12	$3s^23p^53d$	$^1F_3^o$	57.76	58.06	0.31	58.87	1.11	59.06	1.30
13	$3s^23p^53d$	$^1P_1^o$	72.47	72.78	0.31	74.51	2.04	74.58	2.10
14	$3s3p^63d$	3D_1	90.10	90.26	0.16	91.36	1.26	91.48	1.38
15	$3s3p^63d$	3D_2	90.21	90.37	0.17	91.47	1.26	91.60	1.40
16	$3s3p^63d$	3D_3	90.38	90.56	0.18	91.63	1.26	91.80	1.42
17	$3s3p^63d$	1D_2	92.97	93.32	0.35	94.53	1.56	94.47	1.50
18	$3s^23p^4(^3P)3d^2(^3P)$	5S_2		99.75		101.45		102.16	
19	$3s^23p^4(^3P)3d^2(^3F)$	5D_0		100.40		102.17		102.77	
20	$3s^23p^4(^3P)3d^2(^3F)$	5D_1		100.43		102.20		102.81	

21	$3s^2 3p^4 ({}^3P) 3d^2 ({}^3F)$	5D_2	100.48	102.25	102.87
22	$3s^2 3p^4 ({}^3P) 3d^2 ({}^3F)$	5D_3	100.55	102.31	102.96
23	$3s^2 3p^4 ({}^3P) 3d^2 ({}^3F)$	5D_4	100.63	102.39	103.06
24	$3s^2 3p^4 ({}^3P) 3d^2 ({}^3F)$	5F_5	101.67	103.52	104.15
25	$3s^2 3p^4 ({}^3P) 3d^2 ({}^3F)$	5F_4	101.74	103.60	104.22
26	$3s^2 3p^4 ({}^3P) 3d^2 ({}^3F)$	5F_3	101.81	103.69	104.30
27	$3s^2 3p^4 ({}^3P) 3d^2 ({}^3F)$	5F_2	101.85	103.74	104.34
28	$3s^2 3p^4 ({}^3P) 3d^2 ({}^3F)$	5F_1	101.88	103.79	104.38
29	$3s^2 3p^4 ({}^3P) 3d^2 ({}^3F)$	5G_5	103.81	105.87	106.45
30	$3s^2 3p^4 ({}^3P) 3d^2 ({}^3F)$	5G_6	103.92	105.42	106.01
31	$3s^2 3p^4 ({}^3P) 3d^2 ({}^3F)$	5G_4	104.08	106.17	106.74
32	$3s^2 3p^4 ({}^3P) 3d^2 ({}^3F)$	5G_3	104.25	106.37	106.94
33	$3s^2 3p^4 ({}^3P) 3d^2 ({}^3F)$	5G_2	104.35	106.50	106.86
34	$3s^2 3p^4 ({}^3P) 3d^2 ({}^1D)$	3P_0	104.37	106.08	106.58
35	$3s^2 3p^4 ({}^3P) 3d^2 ({}^1D)$	3P_1	104.53	106.25	106.77
36	$3s^2 3p^4 ({}^3P) 3d^2 ({}^1D)$	3P_2	104.63	106.34	107.05
37	$3s^2 3p^4 ({}^3P) 3d^2 ({}^3F)$	3F_2	105.33	107.20	107.65
38	$3s^2 3p^4 ({}^3P) 3d^2 ({}^3F)$	3F_3	105.79	107.68	108.16
39	$3s^2 3p^4 ({}^3P) 3d^2 ({}^3F)$	3F_4	106.11	108.03	108.55
40	$3s^2 3p^4 ({}^3P) 3d^2 ({}^1G)$	3G_5	106.22	108.17	108.68
41	$3s^2 3p^4 ({}^3P) 3d^2 ({}^1G)$	3G_4	106.36	108.32	108.81
42	$3s^2 3p^4 ({}^3P) 3d^2 ({}^1G)$	3G_3	106.77	108.79	109.29
43	$3s^2 3p^4 ({}^3P) 3d^2 ({}^1D)$	3D_3	107.84	109.86	111.32
44	$3s^2 3p^4 ({}^3P) 3d^2 ({}^3F)$	1D_2	107.87	109.76	110.19
45	$3s^2 3p^4 ({}^3P) 3d^2 ({}^1D)$	3F_4	107.91	110.05	110.50
46	$3s^2 3p^4 ({}^3P) 3d^2 ({}^1D)$	3F_3	108.58	110.87	110.28
47	$3s^2 3p^4 ({}^3P) 3d^2 ({}^1D)$	3D_2	108.59	110.81	111.68
48	$3s^2 3p^4 ({}^3P) 3d^2 ({}^3P)$	5D_3	108.86	110.49	110.90
49	$3s^2 3p^4 ({}^3P) 3d^2 ({}^3P)$	5D_2	108.87	110.53	111.24
50	$3s^2 3p^4 ({}^3P) 3d^2 ({}^1D)$	3D_1	108.89	110.95	111.37
51	$3s^2 3p^4 ({}^3P) 3d^2 ({}^3P)$	5D_4	108.92	110.73	111.16
52	$3s^2 3p^4 ({}^3P) 3d^2 ({}^3P)$	5D_1	109.02	110.82	111.23
53	$3s^2 3p^4 ({}^3P) 3d^2 ({}^3P)$	5D_0	109.03	110.90	111.28
54	$3s^2 3p^4 ({}^3P) 3d^2 ({}^1D)$	3F_2	109.07	111.23	110.94
55	$3s^2 3p^4 ({}^1D) 3d^2 ({}^3F)$	3H_4	109.22	111.57	111.93
56	$3s^2 3p^4 ({}^1D) 3d^2 ({}^1D)$	1S_0	109.33	111.12	111.51
57	$3s^2 3p^4 ({}^1D) 3d^2 ({}^3F)$	3H_6	109.41	111.80	112.23
58	$3s^2 3p^4 ({}^1D) 3d^2 ({}^3F)$	3H_5	109.42	111.78	112.18
59	$3s^2 3p^4 ({}^3P) 3d^2 ({}^3P)$	5P_3	109.49	111.44	111.90
60	$3s^2 3p^4 ({}^3P) 3d^2 ({}^3P)$	5P_2	109.59	111.50	111.95
61	$3s^2 3p^4 ({}^3P) 3d^2 ({}^3P)$	5P_1	109.64	111.53	111.95
62	$3s^2 3p^4 ({}^3P) 3d^2 ({}^3P)$	3D_2	110.00	111.99	112.36
63	$3s^2 3p^4 ({}^3P) 3d^2 ({}^3P)$	3D_1	110.11	112.14	112.53
64	$3s^2 3p^4 ({}^1D) 3d^2 ({}^1D)$	1F_3	110.30	113.08	112.75
65	$3s^2 3p^4 ({}^3P) 3d^2 ({}^3P)$	3D_3	110.37	112.35	113.42
66	$3s^2 3p^4 ({}^3P) 3d^2 ({}^3F)$	1G_4	110.57	112.51	112.88
67	$3s^2 3p^4 ({}^1D) 3d^2 ({}^3F)$	3G_3	111.05	112.38	112.71
68	$3s^2 3p^4 ({}^1D) 3d^2 ({}^3P)$	3P_2	111.13	113.11	113.48
69	$3s^2 3p^4 ({}^1D) 3d^2 ({}^3P)$	3P_0	111.18	113.14	113.51
70	$3s^2 3p^4 ({}^1D) 3d^2 ({}^3P)$	3P_1	111.21	113.22	113.60
71	$3s^2 3p^4 ({}^1D) 3d^2 ({}^3F)$	3G_4	111.25	113.20	113.51
72	$3s^2 3p^4 ({}^1D) 3d^2 ({}^3F)$	3G_5	111.63	113.57	113.91
73	$3s^2 3p^4 ({}^1D) 3d^2 ({}^1G)$	1I_6	112.11	115.22	115.60
74	$3s^2 3p^4 ({}^3P) 3d^2 ({}^1G)$	3H_6	112.38	113.53	113.86
75	$3s^2 3p^4 ({}^3P) 3d^2 ({}^1G)$	3H_5	112.46	114.59	114.94
76	$3s^2 3p^4 ({}^3P) 3d^2 ({}^1G)$	3F_2	112.70	114.83	115.10
77	$3s^2 3p^4 ({}^3P) 3d^2 ({}^1G)$	3H_4	112.95	115.10	115.45
78	$3s^2 3p^4 ({}^3P) 3d^2 ({}^1G)$	3F_3	113.01	115.14	115.43
79	$3s^2 3p^4 ({}^1D) 3d^2 ({}^1D)$	1P_1	113.35	115.13	115.40
80	$3s^2 3p^4 ({}^3P) 3d^2 ({}^1G)$	3F_4	113.37	115.50	115.80
81	$3s^2 3p^4 ({}^1D) 3d^2 ({}^1D)$	1G_4	113.58	116.28	116.65
82	$3s^2 3p^4 ({}^3P) 3d^2 ({}^3F)$	3D_1	115.81	118.07	118.38

83	$3s^23p^4(^3P)3d^2(^3F)$	3D_2	115.97	118.30	119.03			
84	$3s^23p^4(^1S)3d^2(^1D)$	1D_2	116.53	118.78	118.57			
85	$3s^23p^4(^3P)3d^2(^3F)$	3D_3	116.81	119.19	119.54			
86	$3s^23p^4(^3P)3d^2(^1S)$	3P_2	117.35	119.31	119.51			
87	$3s^23p^4(^1D)3d^2(^1G)$	1H_5	117.41	119.73	119.94			
88	$3s^23p^54s$	$^3P_2^o$	117.60	120.41	116.82			
89	$3s^23p^4(^1D)3d^2(^3P)$	3F_2	117.63	120.10	120.21			
90	$3s^23p^4(^1D)3d^2(^3P)$	3F_3	117.89	120.38	120.51			
91	$3s^23p^54s$	$^3P_1^o$	117.85	118.20	0.35	121.03	3.18	122.63 4.78
92	$3s^23p^4(^1D)3d^2(^3P)$	3F_4	118.24	120.75	120.89			
93	$3s^23p^4(^3P)3d^2(^1S)$	3P_1	118.39	120.34	120.57			
94	$3s^23p^4(^3P)3d^2(^1S)$	3P_0	118.72	120.68	120.91			
95	$3s^23p^54s$	$^3P_0^o$	119.43	122.33	118.72			
96	$3s^23p^4(^3P)3d^2(^1G)$	3G_4	118.50 ^d	119.61	1.11	123.41	4.91	123.88 5.38
97	$3s^23p^4(^3P)3d^2(^1G)$	3G_5	118.57 ^d	119.63	1.06	123.47	4.90	123.95 5.38
98	$3s^23p^4(^1D)3d^2(^1G)$	3G_3	118.63 ^d	119.69	1.06	123.52	4.89	123.97 5.34
99	$3s^23p^54s$	$^1P_1^o$	119.72	120.03	0.31	122.95	3.23	124.57 4.85

^a NIST [10]

^b Aggarwal *et al.* [13]

^c Storey *et al.* [11]

^d Young [19]

The wave functions of the lowest 17 levels are considered to be most accurate in available calculations, as also noted by Aggarwal *et al.* [13]. The oscillator strengths among these levels should provide overall accuracy of the final residual ionic states. The comparison of oscillator strengths from two GRASP calculations with 1099 levels of the $3s^23p^6$, $3s^23p^53d$, $3s3p^63d$, $3s^23p^43d^2$, $3s3p^53d^2$, $3s^23p^33d^3$, $3s3p^43d^3$, and $3p^63d^2$ configurations of the $n = 3$ complex and with 2471 configurations of the $n = 3$ complex plus additional configurations of the $n = 4$ complex normally agree within about 10%; indicating that the $n = 4$ configurations are less important. We have included in Table II length oscillator strengths and ratios between the length and velocity values from the present work together with the calculations of Aggarwal *et al.* [13] and Verma *et al.* [12]. There are 23 so called dipole-allowed and 15 spin-forbidden transitions possible among these 17 levels. The oscillator strengths for the spin-forbidden transitions are usually smaller than the dipole-allowed transitions as these transitions are induced by the spin-orbit interaction due to mixing of different LS symmetries with the same J and π quantum numbers. The dipole-allowed $3s^23p^6\ ^1S_0 - 3s^23p^53d\ ^1P_1^o$ transition is the strongest transition and our length and velocity values agree to 5%. Our length value agrees within 3% with Aggarwal *et al.* [13] and Verma *et al.* [12].

Next we discuss transitions with oscillator strengths ≥ 0.01 where the agreement between the present length and velocity formulations varies from 19% to 35% with an average difference of about 25%. The results of Aggarwal *et al.* [13] exhibit similar agreement between the length and velocity forms with an overall agreement of about 20% for these transitions. Though the wave functions and CI expansions of Verma *et al.* [12] are deficient as discussed by Aggarwal *et al.* [13], their length and velocity results show on an average 20% difference. The oscillator strengths of Aggarwal *et al.* [13] for this group

of transitions are higher than our results by 20-25%. The calculation of Aggarwal *et al.* [13] is considered to be most extensive and our results for the 2-14, 3-14, 3-15, 4-15, 4-16, and 11-15 transitions are within 20% and differ by about 25% for the remaining transitions. For the weaker transitions with oscillator strengths less than 0.01 all calculations show varied degree of differences between the two forms: on an average about 50%. The agreement between the length and velocity forms to some extent is an indicator of the accuracy of wave functions and the convergence of CI expansions, but it is not necessarily a sufficient condition as demonstrated by several calculations in the past including the work of Aggarwal *et al.* [13]. It is possible that the agreement between the length and velocity values may occur even with very simple wave functions. It may be noted that there is strong interaction between many levels of Fe^{8+} because of the proximity of levels as well as due to the strong interaction between Rydberg series and perturbers. The strong mixing between the levels is sensitive to the choice of wave functions and CI expansions. The cancellations in dipole matrix elements of the main configurations of initial and final states of a transition generally give rise to weaker transitions. The correlation corrections play particularly important role for weaker transitions. Overall agreement of the present oscillator strengths with the GRASP results for transition between all target states of Fe^{8+} is within 20% for the 38% of transitions, and within 50% for the remaining 62% of transitions. These values can be considered as overall estimation of the accuracy of available radiative data for Fe^{8+} .

B. Photoionization calculations

The photoionization calculations have been performed with the B -spline R -matrix (BSR) code [20]. This code

TABLE II: Comparison of oscillator strengths in length formulation and ratios of length and velocity values for transitions between the first 17 levels of Fe⁸⁺ from the present calculation, GRASP calculation by Aggarwal et al. [13], and CIV3 calculation of Verma et al. [12].

Transition	Present		GRASP		CIV3	
	f_L	Ratio	f_L	Ratio	f_L	Ratio
1 3	3.35E-4	0.81	3.70E-4	0.95	3.38E-4	0.47
1 10	5.32E-3	0.77	5.53E-3	0.94	5.56E-3	0.61
1 13	3.07E+0	1.05	3.15E+0	0.96	2.98E+0	0.98
2 14	5.73E-2	1.33	6.95E-2	1.20	5.29E-2	1.10
3 14	1.75E-2	1.35	2.14E-2	1.20	1.62E-2	1.10
3 15	4.04E-2	1.26	4.87E-2	1.20	3.75E-2	1.10
3 17	1.44E-4	1.43	1.55E-4	1.10	1.77E-6	12.0
4 14	1.11E-3	1.40	1.37E-3	1.20	1.03E-3	1.10
4 15	1.22E-2	1.31	1.49E-2	1.20	1.14E-2	1.10
4 16	4.61E-2	1.19	5.51E-2	1.20	4.27E-2	1.10
4 17	2.14E-4	1.52	3.56E-4	0.79	1.44E-4	0.84
5 16	2.98E-2	1.33	4.07E-2	0.68	2.37E-2	0.61
6 15	2.79E-2	1.28	3.79E-2	0.69	2.21E-2	0.61
6 16	1.06E-3	1.02	1.48E-3	0.46	6.95E-4	0.39
6 17	2.21E-4	1.52	4.03E-4	1.00	7.11E-4	0.97
7 14	2.65E-2	1.22	3.59E-2	0.69	2.12E-2	0.59
7 15	1.63E-3	0.98	2.32E-3	0.49	1.14E-3	0.41
7 16	4.93E-6	1.56	8.54E-6	4.10	1.92E-5	21.0
7 17	7.75E-4	1.52	1.12E-3	0.62	7.12E-4	0.68
8 15	1.55E-3	1.40	2.20E-3	1.10	1.66E-3	0.86
8 16	1.88E-2	1.33	2.47E-2	1.00	1.48E-2	0.84
8 17	5.80E-3	1.39	8.07E-3	0.88	5.96E-3	0.77
9 15	8.26E-3	1.20	1.30E-2	0.95	6.29E-3	0.71
9 16	1.04E-3	1.30	2.13E-3	1.00	8.60E-4	0.79
9 17	1.24E-2	1.29	1.68E-2	0.61	9.93E-3	0.55
10 14	1.84E-2	1.27	2.49E-2	1.00	1.53E-2	0.77
10 15	9.80E-3	1.16	1.27E-2	1.10	8.57E-3	0.77
10 17	1.48E-5	1.07	4.43E-5	0.64	9.07E-6	1.00
11 14	1.92E-3	1.31	2.65E-3	1.10	1.62E-3	0.83
11 15	1.13E-2	1.27	1.33E-2	1.00	9.69E-3	0.76
11 16	7.62E-3	1.07	8.83E-3	1.10	6.94E-3	0.76
11 17	5.49E-3	1.24	1.02E-2	0.64	3.56E-3	0.52
12 15	1.78E-5	0.64	1.97E-6	28.0	1.58E-5	0.06
12 16	8.59E-3	1.12	1.20E-2	0.98	8.28E-3	0.70
12 17	1.40E-2	1.20	1.77E-2	0.85	1.11E-2	0.70
13 14	1.58E-5	0.65	1.33E-5	0.94	9.25E-6	0.13
13 15	1.23E-4	0.65	1.01E-4	0.71	2.41E-5	0.23
13 17	6.54E-4	2.15	7.05E-3	0.30	1.64E-3	0.15

employs B -spline Breit-Pauli R -matrix method which was described in details in our previous electron-impact calculations for Fe⁷⁺ [21] and Fe⁶⁺ [22]. The method uses the B -splines as a universal basis to represent the scattering orbitals in the inner region of $r \leq a$. Hence, the R -matrix expansion in this region takes the form

$$\Psi_k(x_1, \dots, x_{N+1}) = \mathcal{A} \sum_{ij} \bar{\Phi}_i(x_1, \dots, x_N; \hat{\mathbf{r}}_{N+1} \sigma_{N+1}) r_{N+1}^{-1} B_j(r_{N+1}) a_{ijk} + \sum_i \chi_i(x_1, \dots, x_{N+1}) b_{ik}. \quad (2)$$

Here the $\bar{\Phi}_i$ denote the channel functions constructed from the N -electron target states, while the splines $B_j(r)$ represent the continuum orbitals. The χ_i are additional

$(N+1)$ -electron bound states. In the standard R -matrix calculations [23], these are included to ensure completeness of the total trial wave function and to compensate for orthogonality constraints imposed on the continuum orbitals. The use of nonorthogonal one-electron radial functions in the BSR method, on the other hand, allows us to completely avoid these configurations for compensating orthogonality restrictions. This procedure has practical advantages in reducing pseudoresonance structure in the scattering solutions (as example, see discussion in Ref. [24]).

The continuum orbitals in the internal region with radius $a = 15 a_0$ were represented with 78 B -splines of order 8 with the maximum interval in this grid of 0.65 a_0 . This is sufficient for a good representation of the scattering electron wave functions for energies up to 200 eV.

The present BSR-99 collision model contained up to 494 scattering channels. In the R -matrix theory, the photoionization cross sections can be defined through the dipole matrix between the initial state Ψ_0 and the R -matrix basis states Ψ_k provided that all radial orbitals of the initial state are well confined in the inner region. The total photoionization cross section for a given photon energy ω is

$$\sigma(\omega) = \frac{8}{3}\pi^2 a_0^2 \alpha \omega^{\pm 1} \frac{1}{(2J_0 + 1)} \sum_j |(\Psi_j^- || D || \Psi_0)|^2 \quad (3)$$

where D is a general dipole operator which could be either the length or velocity operator, and signs (+1) and (-1) correspond to the length and velocity forms. Index j goes over different open channels, and other quantities have their usual meaning. Expanding Ψ_j^- in terms of the R -matrix states, we find that

$$(\Psi_j^- || D || \Psi_0) = \frac{1}{a} \sum_k \frac{(\Psi_k || D || \Psi_0)}{E_k - E_0 - \omega} \mathbf{P}_k^T \mathbf{R}^{-1} \mathbf{F}_j^-(a) \quad (4)$$

where \mathbf{P}_k is the vector of the surface amplitudes for R -matrix solutions Ψ_k , and \mathbf{F}^- is constructed from the solutions in the outer region such that it satisfies the boundary condition

$$\mathbf{F}^- \rightarrow (\pi k)^{-1/2} (\sin \theta + \cos \theta \mathbf{K})(1 + i\mathbf{K})^{-1} \quad (5)$$

corresponding to a Coulomb modified plane wave plus an ingoing spherical wave. The ASYPCK program [25] has been employed to find the asymptotic solutions. The wave functions Ψ_0 in Eq. (4) were taken from our previous calculations of electron scattering on Fe^{7+} [21]. They were obtained in the intensive MCHF calculations and the ground-state ionization potential of 151.05 eV is in excellent agreement with the experimental value of 151.06 eV. Note that it is an independent calculation, with full inclusion of the possible relaxation effects. The ionization threshold for the Fe^{7+} ground state is 151.146 eV from the CI calculation of Sossah *et al.* [7] which is in good agreement with our calculation and experiment.

III. RESULTS

We have attempted to improve theoretical calculations by using an accurate representation of the electron correlation effects both for the Fe^{7+} initial bound levels and the final Fe^{8+} ion plus photoelectron levels in a consistent and balanced manner with non-orthogonal B-spline R -matrix basis functions. The theoretical photoionization calculations have also been improved by including a larger set of residual Fe^{8+} ion levels which were generated within the framework of a combination of MCHF and the B-spline box-based multichannel methods as described above in Section II. The earlier calculation of

TABLE III: Metastable states of Fe^{7+} .

Index	Configuration	LSJ	E (eV)	lifetime (s)
1	$3p^6 3d$	$^2D_{3/2}$	0.00	
2	$3p^6 3d$	$^2D_{5/2}$	0.23	1.10E+01
8	$3p^5 3d^2(^3F)$	$^4G_{11/2}$	51.36	5.90E+02
9	$3p^5 3d^2(^3F)$	$^4G_{9/2}$	51.55	1.86E+00
11	$3p^5 3d^2(^3F)$	$^4G_{7/2}$	51.77	1.02E-04
17	$3p^5 3d^2(^3F)$	$^4F_{9/2}$	53.30	4.36E-02
26	$3p^5 3d^2(^1G)$	$^2H_{11/2}$	55.75	9.79E-01
28	$3p^5 3d^2(^3F)$	$^2G_{9/2}$	56.49	1.54E-02
29	$3p^5 3d^2(^1G)$	$^2H_{9/2}$	56.91	2.52E-02
39	$3p^5 3d^2(^1G)$	$^2G_{9/2}$	60.73	9.05E-03

Sossah *et al.* [7] included 17 levels whereas the present work included 99 levels. The photoionization of a 3p or 3s electron from the Fe^{7+} initial ground configuration $3s^2 3p^6 3d^2 D_{3/2,5/2}$ levels give rise to Fe^{8+} $3s^2 3p^5 3d$ and $3s 3p^6 3d$ levels (1 - 17 levels in Table I). The Fe^{8+} levels of the $3s^2 3p^4 3d^2$ and $3s 3p^5 4s$ configurations (18 - 99 levels in Table I) account for the photoionization process where a photoelectron is ejected and a second electron is promoted to an excited level. The $3s^2 3p^4 3d^2$ levels are also important for photoionization from metastable states discussed below.

The ground initial level of Fe^{7+} is $3s^2 3p^6 3d^2 D_{3/2}$ and the $^2D_{5/2}$ level of ground configuration is a metastable level at 0.228 eV. The $3s^2 3p^5 3d^2$ and $3s^2 3p^6 4s$ configurations also provide many metastable or quasi-metastable levels. The identification of possible metastable levels is very important for interpretation of measured photoionization cross sections because the beam of ions may contain significant population of metastable levels. In particular, metastable states are expected to be present in the primary ion beam of recent measurements of Gharaibeh *et al.* [6] if their lifetimes are comparable to or greater than their flight time in the apparatus ($\sim 10^{-5}$ s). Thus the primary Fe^{7+} ion beam consists of an unknown admixture of ions in the ground level and in metastable levels, and the measured photoions can originate from any of these levels. It may enhance the measured photoion yield spectrum, but it also complicates comparison with theoretical calculations. The systematic calculations of lifetimes for Fe^{7+} levels were provided in our previous calculation [21], and the levels with lifetime more than 10^{-5} are given in Table III. Any of these states may contribute to the photoion yield in measurements of Gharaibeh *et al.* [6].

The photoionization process can occur through direct photoionization where the photon knocks out an electron from the Fe^{7+} ion leaving a residual Fe^{8+} ion. The photoionization can also occur through indirect process where the incident photon excites the ion to autoionizing resonance states that eventually decay by emitting an electron. The former process gives rise to background nonresonant cross sections and latter to series of Rydberg resonances. The present work and the previous TOPbase and BPRM calculations include both processes and the

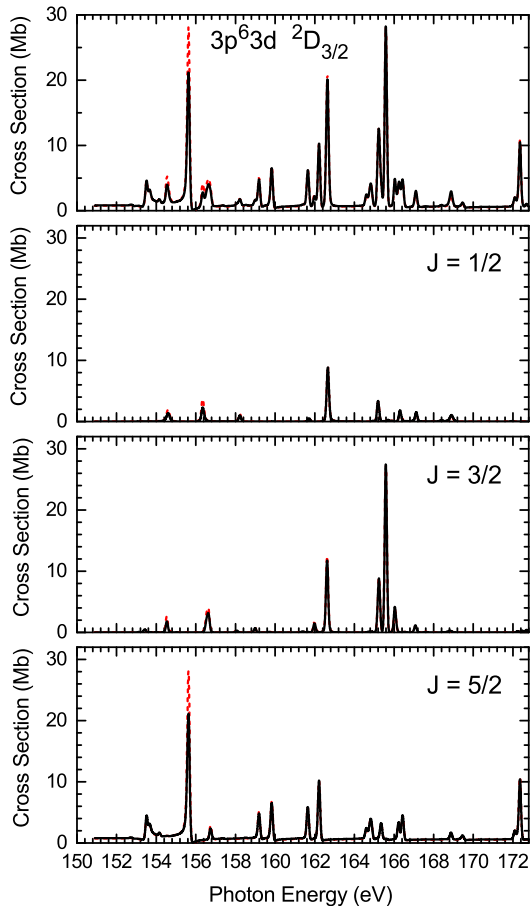


FIG. 1: Present *B*-spline Breit-Pauli *R*-matrix (BSR) cross-sections for photoionization of Fe^{7+} from the ground $3s^23p^63d\ ^2D_{3/2}$ level (top panel) in both length and velocity formulations. The partial photoionization cross sections in both length and velocity forms are shown for $J = 1/2, 3/2, 5/2$ in the lower three panels. Solid (black) curve, length value; dashed (red) curve, velocity value. The cross sections are convoluted with a Gaussian of $\text{FWHM} = 0.126$ eV to simulate the experimental energy resolution.

interference between them. The direct nonresonant photoionization cross sections and the positions and number of resonances from the TOPbase calculation show substantial discrepancies with the measured results. We begin our discussion with the photoionization cross sections from the ground $3s^23p^63d\ ^2D_{3/2}$ level. Our calculation has been carried out across the autoionizing Rydberg series of resonances converging to various residual ionic levels of Fe^{8+} . In the present work we have focused in the photon energy range from ionization threshold to 172 eV where measured cross sections are available. We have calculated partial and total photoionization cross sections for the 3p and 3s subshells of the ground level in both length and velocity formulations. The final $^2P_{1/2,3/2}^o$, $^2D_{3/2,5/2}^o$, and $^2F_{5/2}^o$, that is, $J = 1/2, 3/2, 5/2$ levels are allowed for photoionization from the ground $3s^23p^63d$

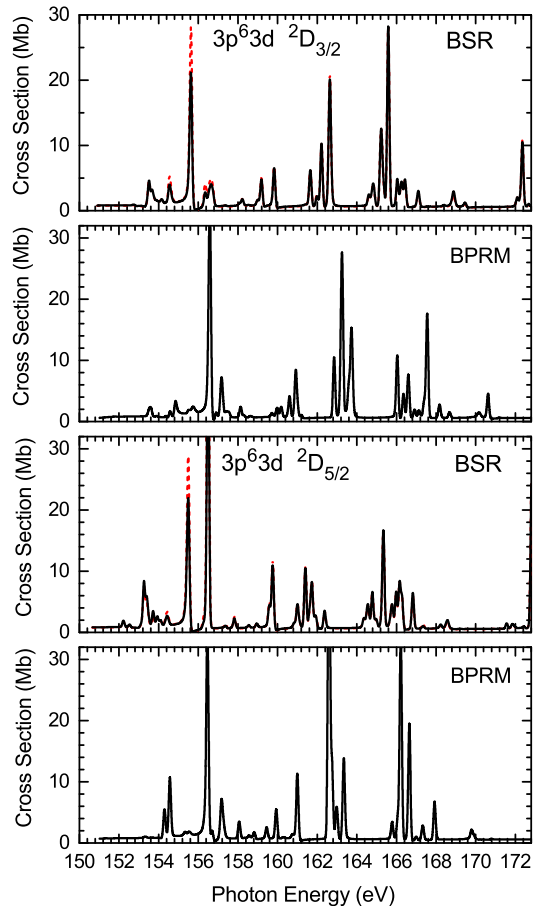


FIG. 2: Comparison of present *B*-spline Breit-Pauli *R*-matrix (BSR) cross-sections in length (solid black curve) and velocity (red dashed curve) forms for photoionization of Fe^{7+} with the Breit-Pauli *R*-matrix (BPRM) calculations [7]. The theoretical cross sections are given for the ground $3s^23p^63d\ ^2D_{3/2}$ and metastable $^2D_{5/2}$ initial states and convoluted with a Gaussian of $\text{FWHM} = 0.126$ eV to simulate the experimental energy resolution.

$^2D_{3/2}^o$ level. The total photoionization cross section is determined by adding partial cross sections for final levels with $J = 1/2, 3/2, 5/2$ which in turn are obtained by combining the channel cross sections. The partial cross sections together with the total photoionization cross sections from the initial ground $3s^23p^63d\ ^2D_{3/2}$ level are displayed in Fig. 1 from the 3p ionization threshold to 172 eV. The lower three panels show the partial cross sections for $J = 1/2, 3/3, 5/2$, respectively, and the top panel gives the total photoionization cross section. The length and velocity results are shown by solid (black) and dashed (red) curves, respectively. There is normally an excellent agreement between the length and velocity forms and this provides some indication that our theoretical results are likely to be accurate. The excitation of 3p electron into Rydberg orbitals produces $3s^23p^53dnl$ and $3s^23p^53dms$ series of Rydberg resonances converging

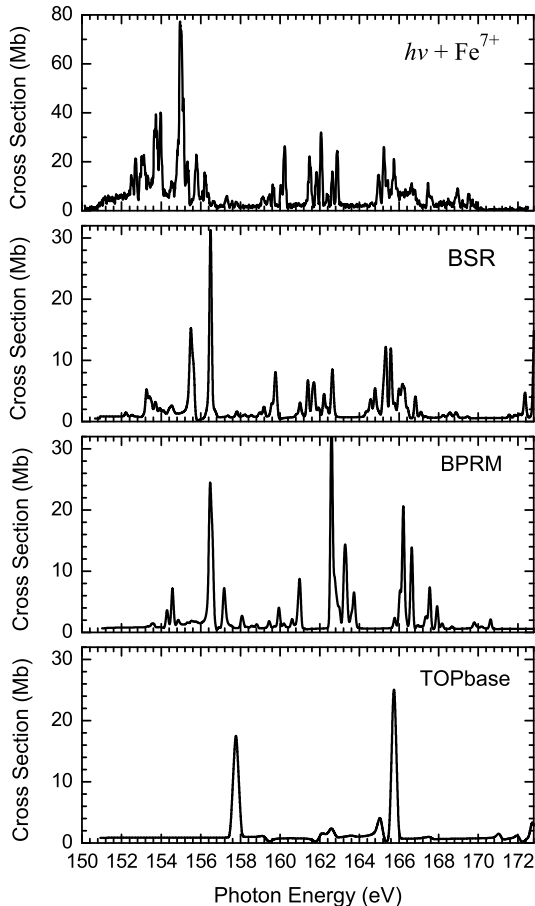


FIG. 3: Comparison of measured absolute cross-section [6] (top panel) for photoionization of Fe^{7+} with the present calculations (BSR), BPRM calculations [7], and the TOPbase theoretical data. Theoretical cross sections are given for the $3s^23p^63d^2D$ initial state and convoluted with a Gaussian of FWHM = 0.126 eV to simulate the experimental energy resolution.

to various Fe^{8+} ionization thresholds. The photoionization cross section shows significant resonance structure with dominant contribution from the $J = 5/2$ partial cross section and weak contribution from the $J = 1/2$ partial cross section. The $J = 5/2$ partial cross section also mostly contributes to the background nonresonant cross section away from resonances. The photoionization cross sections have been calculated at a very fine energy grid of 10^{-4} eV to resolve sharp resonances. The cross sections are then convoluted with a Gaussian of FWHM = 0.126 eV to simulate the experimental energy resolution. The resonances at around 153.6 eV and 155.5 eV in the total cross section are contributed by $J = 5/2$ final levels while the narrow resonance around 165.6 eV arises from the $J = 3/2$ final levels. The other major resonance in the spectrum around 162.5 eV arises due to the combined $J = 1/2$ and $3/2$ final levels and the resonance around 162.2 eV is again due to $J = 5/2$ final levels. The

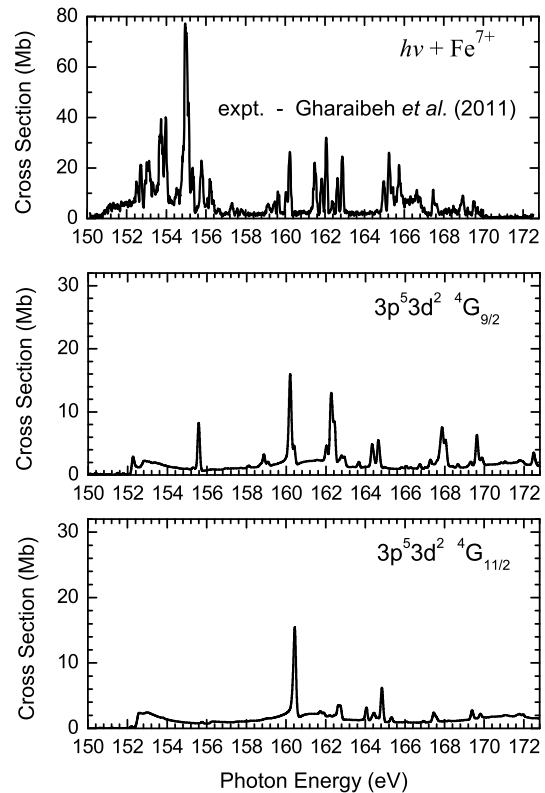


FIG. 4: Comparison of measured absolute cross-section [6] (top panel) for photoionization of Fe^{7+} with the present calculations for the metastable states. Theoretical cross sections are given for the metastable $3s^23p^53d^2\ ^4G_{9/2}$ and $\ ^4G_{11/2}$ initial states and convoluted with a Gaussian of FWHM = 0.126 eV to simulate the experimental energy resolution.

resonances around 155.5 eV, 162.5 eV, and 165.6 eV have magnitude larger than 20 Mb.

We compare the present total photoionization cross sections from the $\ ^2D_{3/2,5/2}$ levels with the BPRM results [7] in Fig. 2. The results are plotted in the photon energy range from 150 eV to 172 eV. Both theoretical cross sections were convoluted with a Gaussian of FWHM = 0.126 eV to simulate the experimental energy resolution. The present results are marked as BSR and the calculations of Sossah *et al.* [7] as BPRM in the panels of Fig. 2. Our BSR results are shown in both length and velocity formulations by solid (black) and dashed (red) curves, respectively. There is excellent agreement between the length and velocity results and the two curves are almost superimposed except for the peak values of the first few resonances where velocity value is larger than the length value. There is generally a good agreement between the two calculations except some shift in position and magnitude of resonances. The discrepancies between the two calculations is caused by the differences in wave functions used in the descriptions of the initial Fe^{7+} bound levels and final continuum levels and residual ionic Fe^{8+} ioniza-

tion thresholds. We have tried to represent both the initial and final levels by accounting for electron correlation effects consistently. The direct nonresonant photoionization cross sections are quite small and there is relatively small interaction between the resonant and nonresonant contributions. Owing to several interacting series of Rydberg resonances, the photoionization cross sections exhibit complex resonance structure. The present cross sections statistically weighted over fine-structure levels of the ground configuration terms are presented in the Fig. 3 together with the TOBbase data and the calculation of Sossah *et al.* [7] obtained in the *LS R*-matrix approach. The top panel of the Fig. 3 shows the measured cross sections [6] and the other three panels display BSR, BPRM, and TOPbase theoretical results. The cross sections contain many resonances due to the $3s^23p^53dnd$ and $3s^23p^53dns$ Rydberg series. The present BSR calculations and the *R*-matrix results of Sossah *et al.* [7] provide richer resonance structure than the TOPbase data. The theoretical positions and number of resonances in the present calculation seem to have improved agreements with measurements relative to BPRM calculation at least in terms of the richness of resonance structures. However, the strengths of resonances differ considerably from the measurements. Integrating the apparent experimental cross section over the energy range from 150 to 172 eV gives an effective oscillator strength of 1.31 ± 0.39 . That should be compared to a theoretical value of 0.31 for the photoionization from the $^2D_{3/2}$ initial state and a value of 0.29 for the photoionization from the $^2D_{5/2}$ initial state. It is evident that any share population of the ground-configuration states will provide cross section approximately with the same strength but different resonance structure. The background cross sections from the three calculations agree very closely. The effective oscillator strength for the TOPbase cross sections in the given energy region is 0.25 and also closely agrees with the present data.

Above comparison shows that the photoionization from the ground-configuration levels cannot explain the difference with experimental absolute normalization. Another possible reason can be considerable population of the other higher excited metastable levels. To check this possibility, we calculated the photoionization cross sections from the $^4G_{9/2}$ and $^4G_{11/2}$ levels which according to the Table III are the most long-living and lowest metastable states from the $3p^53d^2$ configuration. The results are presented in Fig. 4. These cross sections have a little bigger background cross section values but show less intense resonance structure. The effective oscillator strengths for these states over the energy range from 150 to 172 eV are 0.28 and 0.27, respectively. These values are very close to the results for excitation from the ground level. Therefore, the population of these levels in the initial electron beam would not lead to enhancement of the photoion yield. Note that we may expect approximately the same absolute values for the cross sections for photoionization from other terms of the $3p^53d^2$ configu-

ration because they all have close configuration composition. We included 3s, 3p, and 3d ionization channels in our target state expansions. The 3s ionization was found to be very weak relative to the 3p and 3d ionization.

IV. SUMMARY

In this article we presented new detailed calculations of the photoionization of Fe^{7+} from both the ground state and the metastable levels. The calculation of structure and dynamics of 3d open sub-shell ions is a challenging task because of the importance of electron correlation and interchannel coupling effects. The present calculations were motivated partly by considerable diversity of the existing theoretical and experimental data. The calculations were carried out by using *B*-spline *R*-matrix method [20] in the semi-relativistic Breit-Pauli approximation. The multiconfiguration Hartree-Fock method in connection with *B*-spline expansions is employed for an accurate representation of the initial and final levels of Fe^{7+} as well as the residual final target wave functions of Fe^{8+} . The close-coupling expansion for the photoionization continuum includes 99 fine-structure levels of Fe^{8+} which completely cover the energy region under investigation from the threshold to 172 eV. Our photoionization cross sections in length and velocity forms show excellent agreement.

The present background photoionization cross sections agree well with the TOPbase data and with the more recent Breit-Pauli *R*-matrix calculations [7], but show large discrepancies with the experiment. The resonance structure in our calculation shows good agreement with the Breit-Pauli *R*-matrix calculations [7] and to a lesser extent with the TOPbase data. There is a qualitative agreement between the present resonance structure and experiment. The resonance structure in the cross sections from the measurement is more intense and show significant differences in the position and magnitude of resonances with respect to theoretical results. The experimental effective oscillator strengths over the energy range 150 - 172 eV considerably exceeds the calculated values up to a factor of four. The cross sections for photoionization of metastable states were found to have approximately the same magnitude as the cross sections for photoionization of the ground state, thereby, the presence of metastable states in the ion beam can not be the reason for strong enhancement of the measured cross sections. It may also be noted that the measurement was carried out on resonances because of the low values of ion beam current and nonresonant cross section. The uncertainties in the absolute cross section scale in the experiment is estimated to be $\pm 30\%$. The large local concentration of oscillator strengths around 153 eV in the measurement compared to calculated results is perhaps also an indication of normalization error. Based on these findings we can suggest that the experimental normalisation can be in error, and additional measurements

are desirable to resolve the large discrepancies between theory and experiment.

Acknowledgments

This work was supported by NASA under grant NNX11AB62G from the Solar and Heliophysics program

and the United States National Science Foundation under grants PHY-0244470. We thank R. A. Phaneuf and A. M. Sossah for supplying photoionization data in numerical form.

-
- [1] N. R. Badnell, M. A. Bautista, K. Butler, F. Delahaye, C. Mendoza, P. Palmeri, C. J. Zeippen, and M. J. Seaton, *Mon. Not. R. Astron. Soc.* **360**, 458 (2005).
- [2] C. Mendoza, *Comp. Phys. Commun.* **121**, 74 (1999).
- [3] H. Kjeldsen, B. Kristensen, F. Folkmann, and T. Andersen, *J. Phys. B* **35**, 3655 (2002).
- [4] J. M. Bizau, C. Blancard, D. Cubaynes, F. Folkmann, D. Kilbane, G. Faussurier, H. Luna, J. L. Lemaire, J. Blicq, and F. J. Wuilleumier, *Phys. Rev. A* **73**, 020707 (2006).
- [5] N. E. Hassan, J. M. Bizau, C. Blancard, P. Cosse, D. Cubaynes, G. Faussurier, and F. Folkmann, *Phys. Rev. A* **79**, 033415 (2009).
- [6] M. F. Gharaibeh et al., *Phys. Rev. A* **83**, 043412 (2011).
- [7] A. M. Sossah, H.-L. Zhou, S. T. Manson, *Phys. Rev. A* **82**, 043416 (2010).
- [8] O. Zatsarinny and C. Froese Fischer, *Comput. Phys. Commun.* **180**, 2041 (2009).
- [9] C. Froese Fischer, *Comp. Phys. Commun.* **176**, 559 (2007).
- [10] <http://physics.nist.gov/cgi-bin/AtData>.
- [11] P. J. Storey, C. J. Zeippen, and M. Le Dourneuf, *Astron. Astrophys.* **394**, 753 (2002).
- [12] N. Verma, A. K. S. Jha, and M. Mohan, *Astrophys. J. (Suppl.)* **164**, 297 (2006).
- [13] K. M. Aggarwal, F. P. Keenan, T. Kato, and I. Murakamia, *Astron. Astrophys.* **460**, 331 (2006).
- [14] W. Eissner, M. Jones, and H. Nussbaumer, *Comput. Phys. Commun.* **8**, 270 (1974).
- [15] A. Hibbert, *Comput. Phys. Commun.* **9**, 141 (1975).
- [16] K. G. Dyall, I. P. Grant, C. T. Johnson, F. A. Parpia, and E. P. Plummer, *Comput. Phys. Commun.* **55**, 424 (1989).
- [17] M. F. Gu, *Astrophys. J.* **582**, 1241 (2003).
- [18] D. A. Liedahl, Atomic Data Needs for X-ray Astronomy available at <http://heasarc.gsfc.nasa.gov/docs/heasarc/atomic/>.
- [19] P. R. Young, *Astrophys. J.*, **691**, L77 (2009).
- [20] O. Zatsarinny, *Comp. Phys. Commun.* **174**, 273 (2006).
- [21] S. Tayal and O. Zatsarinny, *Astrophys. J.*, **743**, 206 (2011).
- [22] S. Tayal and O. Zatsarinny, *Astrophys. J.*, **788**, 24 (2014).
- [23] P. G. Burke, *R-Matrix Theory of Atomic Collisions*, Springer-Verlag (Berlin, Heidelberg, 2011).
- [24] S. S. Tayal and O. Zatsarinny, *Phys. Rev. A* **78**, 012713 (2008).
- [25] M. A. Creeves, *Comput. Phys. Commun.* **19**, 103 (1980).